ELSEVIER

Spectrochimica Acta Part B 57 (2002) 1713–1725

SPECTROCHIMICA ACTA PART B

www.elsevier.com/locate/sab

Studies on laser defocusing effects on laser ablation inductively coupled plasma-atomic emission spectrometry using emission signals from a laser-induced plasma

Masaki Ohata[a], Yoshihiro Iwasaki[a], Naoki Furuta[a,*], Isaac B. Brenner[b]

[a]*Faculty of Science and Engineering, Department of Applied Chemistry, Chuo University, 1-13-27, Kasuga, Bunkyou-ku, Tokyo 112-8551, Japan*

[b]*Environmental Analytical Laboratory, Analytical Laboratory, BGU, 9 Dishon Street, Malkha, Jerusalem 96956, Israel*

Received 6 May 2002; accepted 12 August 2002

Abstract

The effect of laser defocusing on analytical performance of laser ablation inductively coupled plasma atomic emission spectrometry (LA-ICP-AES) was studied by varying laser focus conditions with respect to the surface of a low-alloy steel and a powdered sediment pellet. Laser-induced plasma (LIP) and LA-ICP-AES emission signals and LIP excitation temperatures (LIP T_{ex}) were determined and compared for different laser defocus conditions. LIP Fe and LA-ICP-AES Fe emission signals and LIP T_{ex} decreased when the laser was defocused for the low-alloy steel. On the other hand, when the sediment pellet was ablated, LIP T_{ex} decreased when the laser was defocused. However, LA-ICP-AES Fe emission signals increased at first, then decreased when the laser was defocused more. It was concluded that LIP T_{ex} and LIP and LA-ICP-AES Fe emission signals are dependent on laser shot conditions (focus–defocus), and are also dependent on sample type (texture, mineralogy, hardness, conductivity and heat capacity).

Keywords: Laser defocusing; Laser power density; Laser-induced plasma; Excitation temperature; Laser ablation inductively coupled plasma atomic emission spectrometry

1. Introduction

Laser ablation (LA) coupled to inductively coupled plasma atomic emission (LA-ICP-AES) [1–8] and mass spectrometry (LA-ICP-MS) [9–19] has become widespread for determination of trace elements in solid samples. There are several advantages of LA compared to conventional solution nebulization, i.e. rapid bulk analysis with minimum sample preparation, spatial analysis [9,13,15–17] and depth profiling [1,2,12,18,19]. On the other hand, in liquid sample preparation, tedious decompositions have to be performed, and consequently, there is a potential for contamination from reagents and loss of volatile analytes. Thus, LA-ICP-AES and MS have been widely applied for analysis of

*Corresponding author. Tel.: +81-3-3817-1906; fax: +81-3-3817-1895.

E-mail address: nfuruta@chem.chuo-u.ac.jp (N. Furuta).

0584-8547/02/$ - see front matter
PII: S0584-8547(02)00139-8

glass [4,5,10,19], ceramics [1,2,7,12,18], polyvinyl chloride (PVC) [3,6] and environmental samples such as bark [16], plants [14], shells [15] and geological samples [8,9,11,13].

However, LA has several disadvantages. Precision is degraded compared to that of the ICP-AES and MS with conventional solution nebulization. Several workers have investigated the sources of signal variations in LA-ICP-AES [20–25] and MS [26–30]. Poor analytical precision has been attributed to shot-to-shot laser power fluctuations, heterogeneous chemical composition, textural variations [20] and different vaporization for analytes and matrix [21–23,25–30]. The latter produces components commonly designated as fractionation.

Laser properties using laser-induced plasma (LIP) emission spectra and various applications have also been reported [31–39]. These studies facilitate the understanding of ablation mechanisms. A study of the behaviors of analytes in the laser plume vs. their behavior in the plasma will undoubtedly throw light on complex processes and also focus efforts on unanswered aspects of ablation and particle atomization. From LIP excitation temperatures (LIP T_{ex}) and electron number densities, interaction between laser plume and sample surface can be elaborated. As a result, analytical performance can be improved.

In our recent investigations, we observed that the trend of LA-ICP-AES signals for low-alloy steel was different from pellet samples when laser shot conditions changed. For low-alloy steel samples, in-focus laser shot conditions produced the highest intensity. On the contrary, for pellet samples, defocused laser shot conditions gave higher LA-ICP-AES signals.

In order to investigate the ablation behavior for different solid samples, a certified low-alloy steel and a pond sediment pellet were selected as solid samples in this study. Fe emission signals in LIP and LA-ICP-AES were measured and compared for different solid samples and for different laser focus conditions. For the investigation of different LIPs, LIP T_{ex} was also measured and compared for different solid samples and for different laser focus conditions.

2. Experimental

Fig. 1 shows the schematic configuration of the system used in this study. LA and ICP-AES operating conditions are listed in Table 1. The carriage system has two parallel cylindrical stainless rails, whose horizontal position can be adjusted accurately. The LA instrument, installed on the rail system, was an LSX-100 LA system (Cetac, Omaha, USA), employing a TEM_{00} UV Nd:YAG laser with near Gaussian beam profile. This laser was operated at a repetition rate of 20 Hz. A quartz sample cell (45 cm^3) was used [40]. An adjustable $X–Z$ stage facilitated measurement of LIP emission signals at different focus–defocus positions, while varying the Z positions of the sample cell.

The sample surface was moved with respect to the laser focusing point (0, $\pm$1, $\pm$2, $\pm$3, $\pm$5 and $\pm$7 mm). A lens (45 mm diameter, 170 mm focal length) and optical fiber (core diameter of 0.8 mm, Mitsubishi Cable Industries, Ltd, Japan) was installed on the $X–Z$ stage as shown in Fig. 1. A He–Ne laser was installed on the rail system for parallel and horizontal adjustments and alignment of the optical lens for collecting LIP emission signals. The optical lens was located so that the laser plume was magnified by a factor of 2. Since the core diameter of the optical fiber was 0.8 mm, emission signals corresponded to a 0.4 mm diameter of the LIP. For in-focus, the width of the LIP was approximately 1–2 mm and the height 2–3 mm. Size decreased with increasing the laser defocus. The $X–Z$ stage was adjusted so as to obtain maximum LIP emission intensity for each laser focus condition. Therefore, the observation position was approximately 0.3–0.5 mm above the surface of the sample with in-focus condition, and just above the surface with defocus conditions.

The emission collected by the optical fiber was dispersed by a holographic grating (2400 grooves mm^{-1}) mounted in a monochromator (HR 1000, Jobin Yvon–Horiba, France). Radiation was detected by a photomultiplier tube (PMT: Model R919, Hamamatsu Photonics, Hamamatsu, Japan) or by an intensified self-scanning photodiode array detector (ISPD: Model 1421, EG and G Princeton Applied Research, Princeton, NJ). A PMT was employed for the measurement of LIP Fe I 373.5

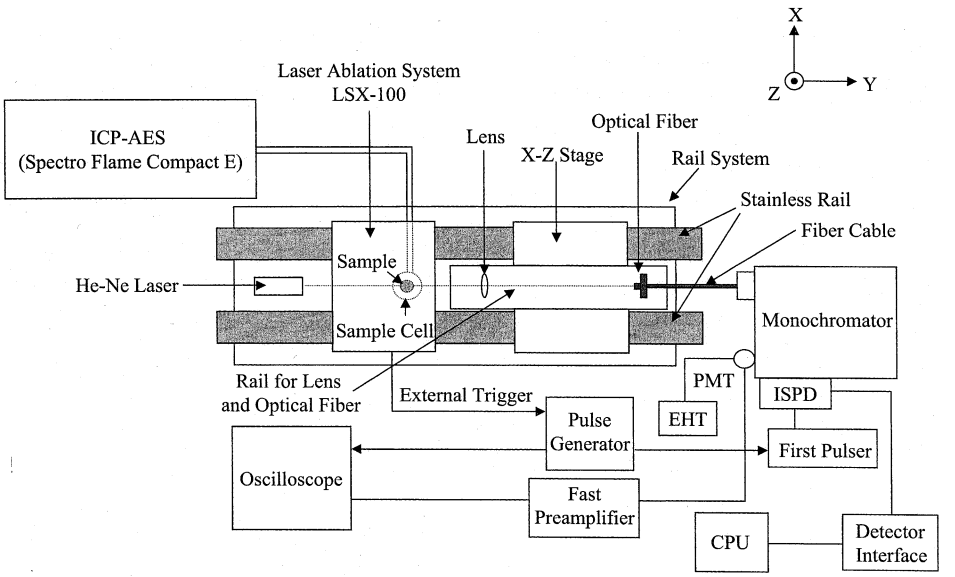

Fig. 1. Schematic diagram of the instrument configuration used for measuring LIP emission and LA-ICP-AES.

nm emission intensity. For time-resolved LIP T_{ex} measurements, six Fe I lines (368–378 nm) were detected simultaneously by the gated-ISPD (20 ns gate width). PMT signals were introduced into a fast preamplifier (Model SR 240, Stanford Research Systems, CA, USA), and converted from current to voltage and amplified. LIP emission signals were also observed on an oscilloscope (TDS 360, Tektronix Inc., Beaverton, OR). The oscilloscope has a function to save signals and later integrated emission signals can be calculated. When ablation commenced, an external trigger, generated from the LA system (LSX-100), was introduced into a digital pulse generator (Model DG 535, Stanford Research Systems). The trigger was also introduced into the oscilloscope via a digital pulse generator for defining the start time (0 ns for delay time) of the laser shot and also for determining the measurement time of LIP emission signals. The delay time of the gated-ISPD detection was controlled by the digital pulse generator, thus facilitating measurement of time-resolved LIP T_{ex}. The output energy (2.1 ± 0.1 mJ) and shot frequency (20 Hz) of the laser were constant during all experiments. Focus conditions varied from 0 to ± 7 mm by moving the sample surface with respect to the laser focusing point. The laser pulse duration of 8 ns was also fixed. Consequently, power densities could be changed for each laser focus condition. LA was conducted in the raster mode. Therefore, laser power densities could be fixed during experiments using different focus conditions.

The low-alloy steel standard (JSS 1008, Japanese Iron and Steel CRMs, Iron and Steel of Japan, Tokyo, Japan) and a pellet prepared from the pond sediment (SRM NIES-2, National Institute for Environmental Studies, Tsukuba, Japan) were used for evaluation of LIP and LA-ICP-AES Fe emission signals and LIP T_{ex}. The chemical composition of the latter is—oxygen approximately 50, Si 21, A1 10.6, Fe 6.53%; original grain size <71 μm (<200 mesh). A sample of the pond sediment weighing 0.2 g was pelletized for 30 min at 30 MPa. The diameter of the pellet was 10 mm and approximately 2 mm thick.

LA-ICP-AES Fe I 373.5 nm emission signals were measured by using a Spectro Flame Compact E (Spectro. Co. Ltd, Kleve, Germany) ICP-AES instrument coupled to the LA. The LA cell was connected to the ICP by a 3 m Tygon tube (1/8 in. i.d.). The ablation time of 30 s was fixed, i.e.

Table 1
Operating conditions of LA systems and ICP-AES

LA system	LSX-100 (Cetac)
Laser	Nd:YAG
Laser mode	Q-switched
Wavelength	266 nm
Pulse duration	8 ns
Output energy	2.1 ± 0.1 mJ
Frequency	20 Hz
Measurement systems for emission signals from LIP	
Optical fiber	(Mitsubishi Cable Industries, Ltd)
Diameter	800 μm
Monochromator	HR-1000 (Jobin Yvon)
Focal length	1000 mm
Grating	2400 grooves mm^{-1}
Slit height of entrance and exit	7 mm
Slit width of entrance and exit	50 μm
Pulse generator	Model DG 535 (Stanford Research Systems)
Delay time from laser pulse	0–4000 ns
Detector for Fe I 373.5 nm emission signal measurement from the LIP	
Photomultiplier tube	R 919 (Hamamatsu Photonics)
High voltage power supply	Model PS 325 (Stanford Systems, Inc.)
Fast preamplifier	Model SR 240 (Stanford Research Systems)
Oscilloscope	TDS 360 (Tektronix)
Detector for excitation temperature measurement of the LIP	
Intensified self-scanning photodiode array detector	Model 1421 (EG&G Princeton Applied Research)
Gate width	20 ns
Detector interface	Model 1461 (EG&G Princeton Applied Research)
Fast pulser	Model 1302 (EG&G Princeton Applied Research)
ICP-AES	*Flame Compact E* (Spectro)
Incident power	1.2 kW
Plasma gas flow rate	16.0 l min^{-1}
Auxiliary gas flow rate	1.26 l min^{-1}
Carrier gas flow rate	0.77 l min^{-1}

600 laser pulses (20 Hz) per measurement, for measurement of LA-ICP-AES Fe emission signals with time-resolved analysis mode.

3. Result and discussions

3.1. Laser power density estimation

Crater diameters for a focused laser are smaller than those for a defocused laser when the laser output energy is constant. Therefore, laser power densities will vary when focus changes. Because laser power densities cannot be determined for each laser defocus condition, they were estimated from low-alloy steel crater diameters. In addition, laser power densities vary for different sample types (composition, hardness, conductivity, heat capacity) because crater diameters change for different types of solid samples even when similar laser shot conditions are used. Low-alloy steel was selected for this defocus experiment, because it was considered that crater diameters would be controlled to a larger extent by laser power density than in the case of the pellet.

Fig. 2 shows laser power densities calculated from observed crater diameters of the low-alloy steel for each laser defocus position. Crater diameters, indicated at each laser position, were determined using a CCD camera installed for the LA system and its operating software. Power density decreased sharply from 37 GW cm^{-2} in-focus to

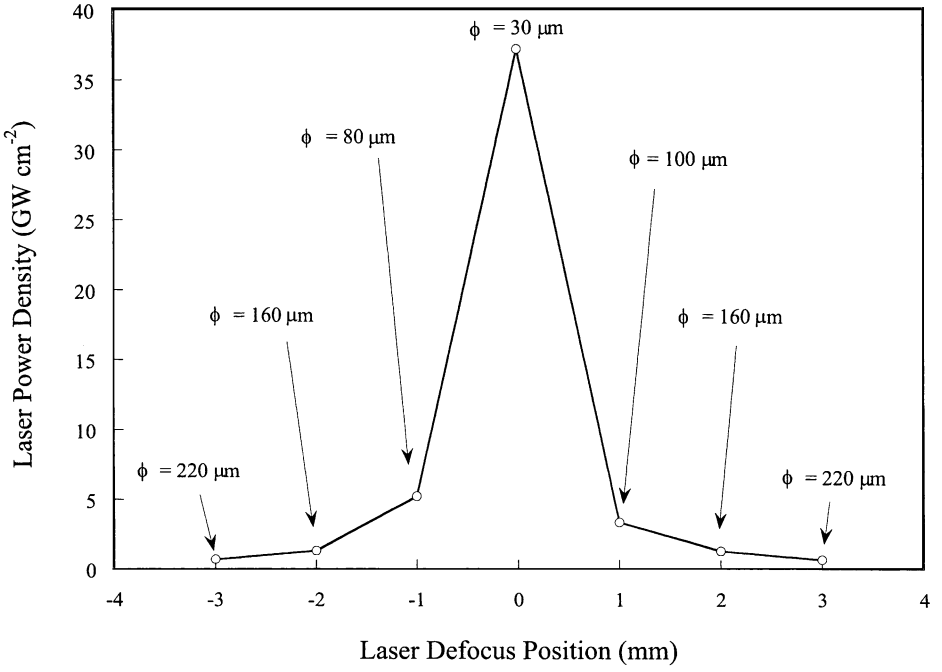

Fig. 2. Estimated laser power density of the LA system as a function of laser defocus position. This was estimated using a certified low-alloy steel sample. Crater diameters for each laser defocus position are also indicated. The laser output energy was constant at 2.1 ± 0.1 mJ during all experiments.

4 GW cm^{-2} at ± 1 mm from the in-focus position. Approximate crater diameters were determined for the sediment; they were larger than those of the low-alloy steel for the same laser focus conditions. They were approximately 50–100 μm and several hundred micrometer for in-focus and defocus conditions, respectively.

3.2. LIP Fe I 373.5 nm emission signals for low-alloy steel and pond sediment

In order to evaluate the effect of laser defocusing, LIP Fe I 373.5 nm emission signals were measured for the low-alloy steel and the pond sediment pellet (Fe content >99 and 6.53%, respectively). Fig. 3 shows LIP Fe emission signals for the low-alloy steel observed on the oscilloscope. LIP Fe emission signals obtained from the pond sediment pellet are shown in Fig. 4. Only results obtained for positive defocus conditions are shown in Figs. 3 and 4, because trends for negative defocus were similar.

The high voltage power supply of the PMT was −500 and −600 V for the low-alloy steel and the pond sediment pellet, respectively. In both cases, LIP Fe emission signals were observed with 0, ± 1, ± 2 and ± 3 mm laser defocus conditions. In the case of the low-alloy steel (Fig. 3), the maximum LIP Fe emission intensity was obtained when the laser was in-focus. LIP Fe emission signals decreased sharply when the laser was defocused. Moreover, the delay time of the LIP Fe emission signal peak decreased when the laser was defocused. In addition, the signal was broader. On the other hand, the trend for the pond sediment pellet was different. Fig. 4 shows that LIP Fe emission signal for +1 mm was similar to that for in-focus. LIP emission intensities observed for +1 and +2 mm laser defocus did not significantly differ from that observed in-focus. Delay times of LIP Fe emission signal peaks decreased when the laser was defocused.

Fig. 5a–d show the LIP Fe relative intensities for both the low-alloy steel and pond sediment

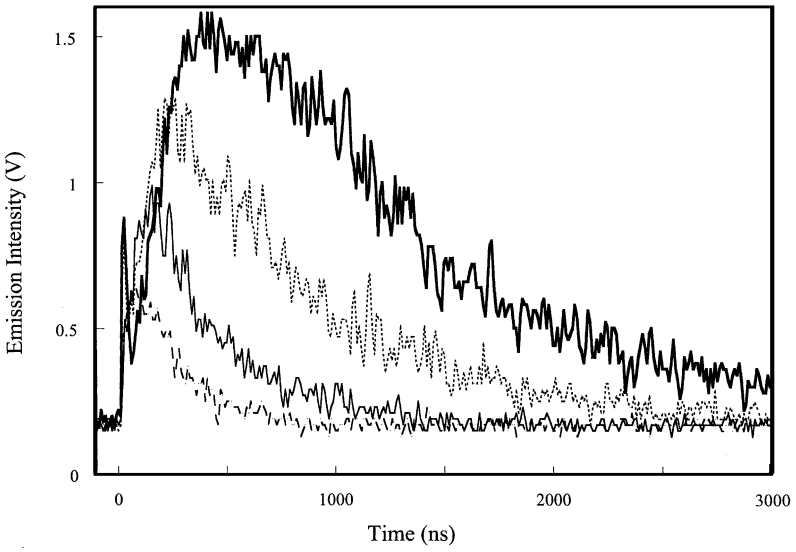

Fig. 3. LIP Fe I 373.5 nm emission signals for in-focus and positive laser defocus positions for low-alloy steel. 0 mm (—); +1 mm (-----); +2 mm (—); +3 mm (– –). LIP Fe emission signals were measured using a PMT. The high voltage was −500 V during these measurements.

pellet for positive laser defocus positions. These relative intensities were normalized to the LIP emission intensity observed at 0 ns. From Fig. 5, it can be seen that relative LIP Fe intensities for the low-alloy steel were slightly larger and persisted for a longer period than those for the pond

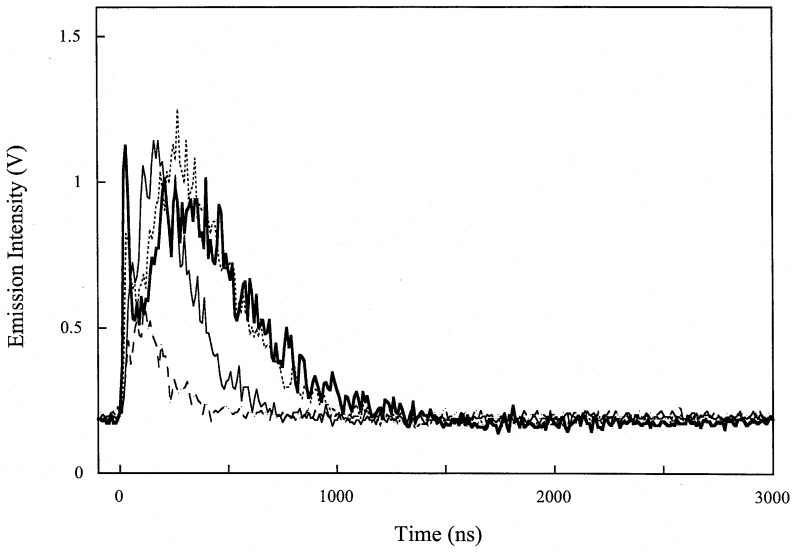

Fig. 4. LIP Fe I 373.5 nm emission signals for in-focus and positive laser defocus positions for NIES pond sediment pellet. 0 mm (—); +1 mm (-----); +2 mm (—); +3 mm (– –). LIP Fe emission signals were measured using a PMT. The high voltage was −600 V during these measurements.

sediment. In particular, in the focus condition, difference of the relative LIP Fe intensities was large compared to that of other defocus conditions.

From these results, it can be concluded that the lifetime of the LIP for the low-alloy steel differed from that for the pond sediment pellet. Relative LIP Fe intensity for the low-alloy steel decreased with increasing laser defocus. In comparison to other laser conditions, the change of intensity between in-focus and +1 mm defocus was larger. On the other hand, relative LIP Fe intensity for the pond sediment did not change significantly from in-focus to +2 mm. It can be considered that whereas low-alloy steel was affected by laser power density changes such variations were not observed for the pond sediment pellet. The larger area ablated with defocus seems to compensate for the decrease of laser power densities for the pond sediment pellet.

3.3. LIP T_{ex} for low-alloy steel and pond sediment

On the bases of the data presented in Section 3.2, it can be concluded that the LIP produced from low-alloy steel differed from that formed from pond sediment. Different LIP T_{ex} for the different samples result in different LIP Fe emission signals. Consequently, LIP T_{ex} was determined using both types of samples. LIP T_{ex} determined for different delay time using the gated-ISPD, was calculated using procedures described elsewhere [31–33,41]. Six Fe I atom lines 371.9, 373.5, 373.7, 374.6, 375.0 and 375.8 nm were employed. Assuming local thermodynamic equilibrium, the slope of the linear regression through the Boltzmann plot was related directly to LIP T_{ex}. Figs. 6 and 7 show time-resolved LIP T_{ex} obtained for the low-alloy steel and the pond sediment pellet, respectively. In Figs. 6 and 7, only positive defocus positions of LIP T_{ex} are plotted because negative positions showed the similar T_{ex} trends. Precision of LIP T_{ex} measurements was approximately 7–10%. In both cases, maximum LIP T_{ex} was obtained when the laser was focused with respect to the sample surface. The highest excitation temperatures of approximately 10 000 K were observed only for a short period of time. When the laser was defocused, LIP T_{ex} decreased both for the low-alloy steel and the pond sediment pellet (Figs. 6 and 7). It should be noted that the LIP T_{ex} of the low-alloy steel was observed for a longer period. The high LIP T_{ex} for the low-alloy steel in-focus position persisted for a longer period. The difference between LIP T_{ex} for in-focus and defocus positions is illustrated in Fig. 6. On the other hand, the trend of LIP T_{ex} for the pond sediment pellet was different (Fig. 7). In this case, LIP T_{ex} substantially decreased with time.

From these results, it can be concluded that LIP T_{ex} depends on laser shot conditions and on sample type. It can be considered that the LIPs obtained for low-alloy steel differ from that measured for the pond sediment. The difference is attributed to sample composition, hardness, conductivity and heat capacity. The low-alloy steel has larger conductivity and heat capacity compared to that of the pond sediment pellet. Therefore, it can be considered that the high LIP T_{ex} of the low-alloy steel will be maintained for longer times compared to those of the pond sediment.

3.4. Evaluation of LA-ICP-AES Fe emission intensities for low-alloy steel and pond sediment

Fig. 8 shows LA-ICP-AES Fe I 373.5 nm intensities as a function of defocus positions from −7 to +7 mm. In the case of the low-alloy steel, the highest Fe emission intensity was observed when the laser was in-focus and intensities decreased when the laser was defocused. In the case of the pond sediment, LA-ICP-AES Fe intensities were enhanced when the laser was defocused (±2 and ±3 mm). Fe emission intensities decreased with increasing laser defocus positions. Hemmerlin et al. [3] observed a similar laser defocusing effect with a PVC. They measured LA-ICP-AES C and Ti signals from the PVC for different laser focus conditions (−2 to +2 mm), and noted that signals were enhanced with laser defocus conditions. Taking into account, sample hardness, conductivity and heat capacity, it can be concluded that the trends for the pond sediment pellet were similar to those of PVD. From these results, it can be concluded that the defocusing effect on LA-ICP-AES Fe emission intensities of

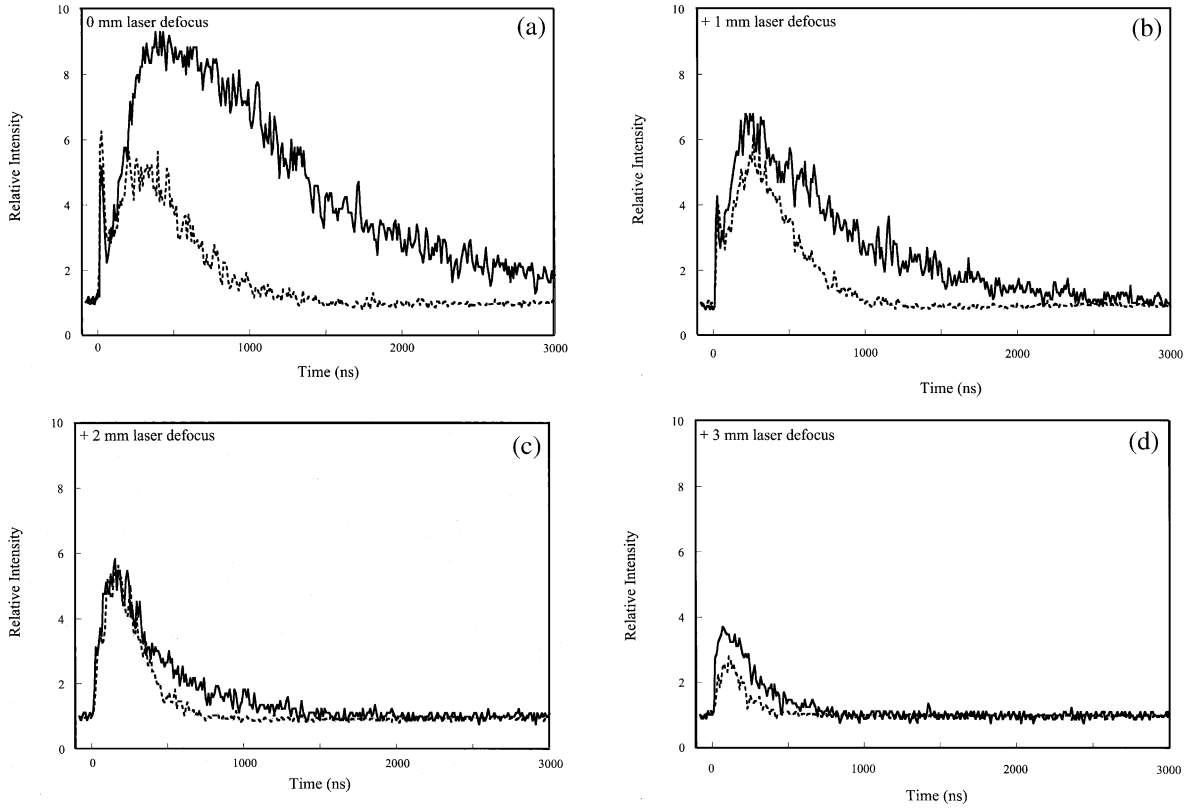

Fig. 5. (a) Relative LIP Fe intensities for the low-alloy steel and pond sediment pellet in-focus laser position. Low-alloy steel (—), pond sediment pellet (----). (b) As in (a) +1 mm laser defocus position. (c) As in (a) +2 mm laser defocus position. (d) As in (a) +3 mm laser defocus position.

low-alloy steel differed from that of the pond sediment pellet.

It is worth noting that LA-ICP-AES Fe intensities for the pond sediment pellet (6.53% Fe) were larger than those for low-alloy steel (>99% Fe). Despite the very large differences in Fe content, LA-ICP-AES Fe emission intensities for in-focus were similar. In defocus, Fe emission intensities were five- to tenfold larger than those of the low-alloy steel. Results obtained here could be explained by the difference of sample properties. Because hardness, conductivity and heat capacity of the pond sediment pellet are low compared to those of the low-alloy steel, crater diameters and the ablated amount for pond sediment pellet was larger than that for low-alloy steel. On the basis of these observations, it can be concluded that the ablation efficiency for the pellet exceeded that for low-alloy steel.

Figs. 9 and 10 show relative LIP Fe and LA-ICP-AES Fe emission intensities for low-alloy steel and pond sediment pellet, respectively. The net LIP Fe I 373.5 nm signal was calculated by subtracting the LIP continuum Fe I 373.0 nm signal from the gross emission signal. Relative emission intensities were normalized relative to the in-focus net integrated emission intensity. Only positive defocus positions are illustrated because negative positions have similar trends. Fig. 9 shows that the relative Fe intensities for the steel LIP and LA-ICP-AES decreased and were similar in trend with increasing laser defocus position. On

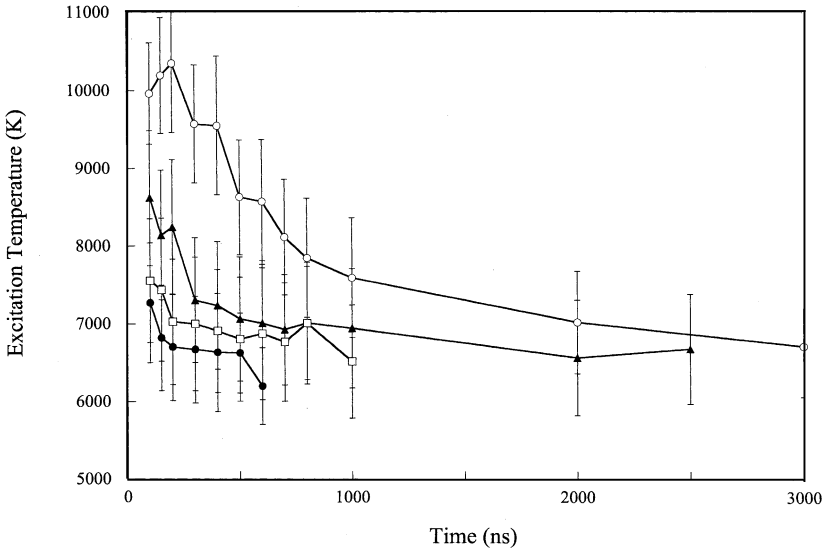

Fig. 6. LIP T_{ex} for different laser defocus positions for low-alloy steel. 0 mm (–○–); +1 mm (–▲–); +2 mm (–□–); +3 mm (–●–). Error bars indicate ±1 SD calculated from the deviation from a linear regression curve of a Boltzmann plot.

the other hand, the trend for pond sediment LIP Fe and LA-ICP-AES Fe emission intensities was different (Fig. 10).

From these observations, it can be concluded that low-alloy steel LIP T_{ex} and Fe emission intensities are closely related and are dependent

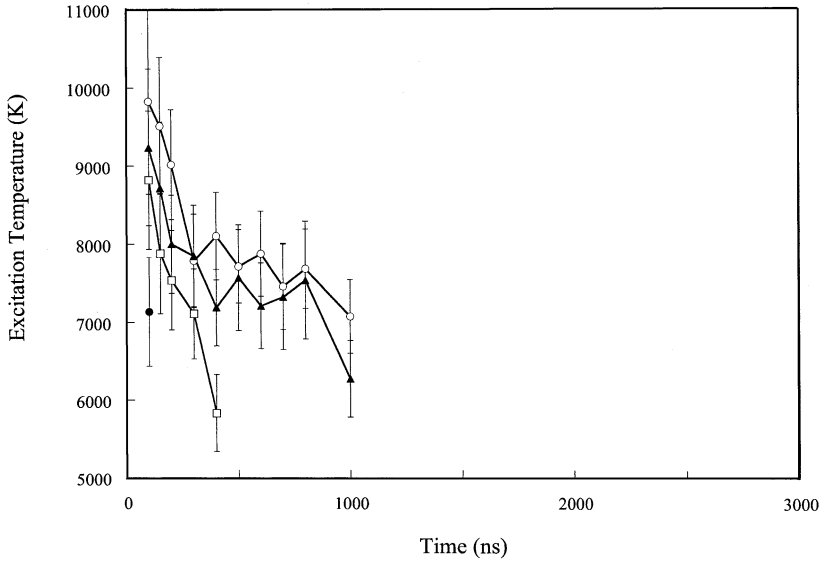

Fig. 7. LIP T_{ex} for different laser defocus positions for pond sediment pellet. 0 mm (–○–); +1 mm (–▲–); +2 mm (–□–); +3 mm (–●–). Error bars indicate ±1 SD calculated from the deviation from a linear regression curve of a Boltzmann plot.

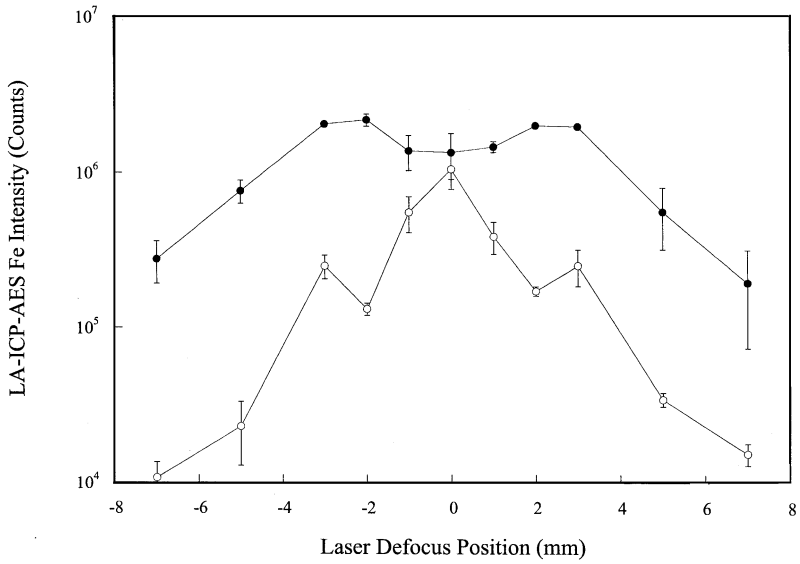

Fig. 8. LA-ICP-AES Fe I 373.5 nm intensities for low-alloy steel and pond sediment as a function of laser defocus position. Low-alloy steel (–○–), pond sediment pellet (–●–). Error bars indicate ±1 SD ($n=3$).

on laser power densities. On the other hand, in the case of pond sediment the relation is more complex. Evidently, there is no distinct association between LIP Fe and LA-ICP-AES Fe emissions. The efficiency of pond sediment ablation was greater than that of low-alloy steel. In the case of pond sediment, shock and stress waves might be an important factor.

Although the LIP T_{ex} decreased with increasing laser defocus, LA-ICP-AES Fe signal intensities

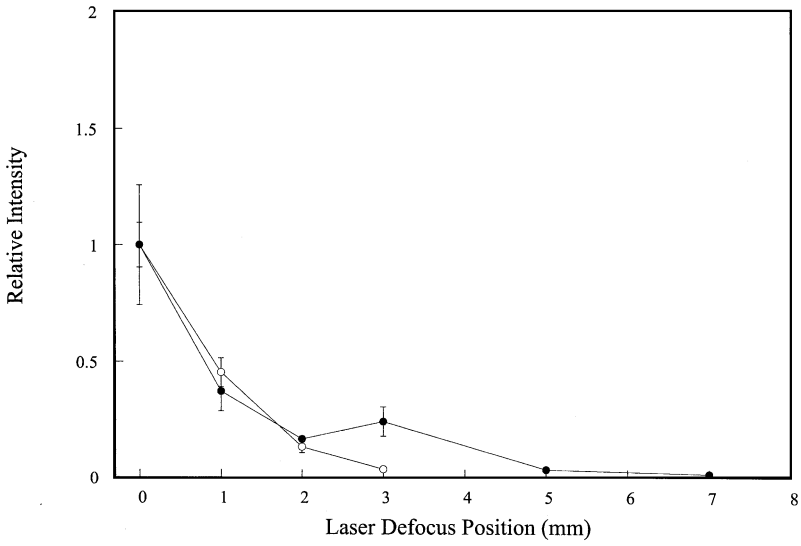

Fig. 9. Relative Fe intensities for LIP and LA-ICP-AES for low-alloy steel as a function of laser defocus position. LIP Fe (–○–), LA-ICP-AES Fe (–●–). Error bars indicate ±1 SD ($n=3$).

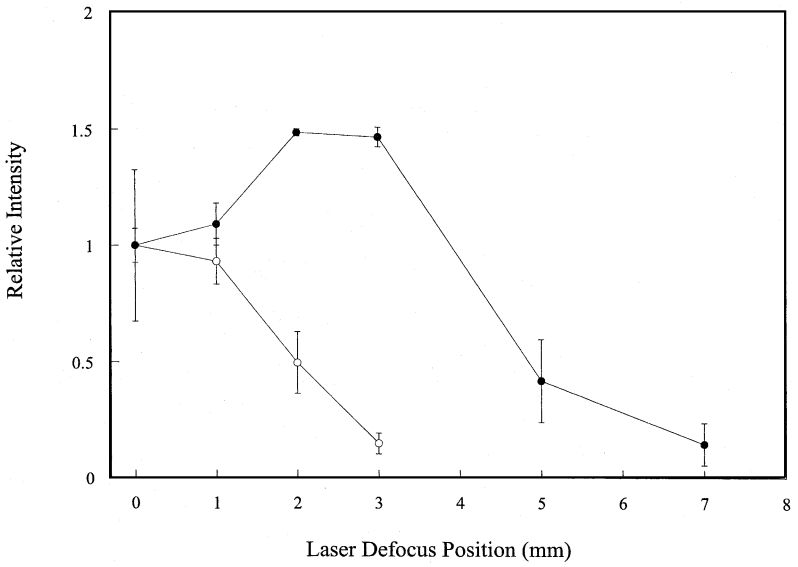

Fig. 10. Relative Fe intensities for LIP Fe and LA-ICP-AES for pond sediment as a function of laser defocus position. LIP Fe (–○–), LA-ICP-AES Fe (–●–). Error bars indicate ±1 SD ($n=3$).

were enhanced due to the increase in the efficiency of ablation for the pond sediment. This is attributed to structural and textural characteristics and possibly labile forms of Fe mineral species. Mechanical processes involving explosive eruption by shock waves producing large amounts of material should also be taken into account.

4. Conclusions

The effect of laser defocus–focus was evaluated using low-alloy steel and a pond sediment pellet. Fe emission signals in the LIP and the LA-ICP-AES for these samples behaved differently in response to laser focus and defocus positions. LIP T_{ex} was dependent on laser focus-defocus and also on sample type. Low-alloy steel was influenced by laser power density variation and it can be concluded that ablation mechanisms for low-alloy steel was dependent on laser power density. This is explained by rigid crystalline textures, high conductivity and heat capacity. On the other hand, structural and textural characteristics, labile forms of Fe mineral species and possibly explosive eruption by shock waves are mechanisms prevail when pressed sediment pellets are ablated.

References

[1] V. Kanicky, J. Musil, J.M. Mermet, Determination of Zr and Ti in 3-μm-thick ZrTiN ceramic coating using laser ablation inductively coupled plasma atomic emission spectrometry, Appl. Spectrosc. 51 (1997) 1037–1041.

[2] V. Kanicky, I. Novotny, J. Musil, J.M. Mermet, Depth profiling of thick layers of graded metal-zirconia ceramic coating using laser ablation inductively coupled plasma atomic emission spectrometry, Appl. Spectrosc. 51 (1997) 1042–1046.

[3] M. Hemmerlin, D. Somas, C. Dubuisson, F. Loisy, E. Poussel, J.M. Mermet, Bulk analysis by IR laser ablation inductively coupled plasma atomic emission spectrometry, Fresenius J. Anal. Chem. 368 (2000) 31–36.

[4] M. Ducreux-Zappa, J.M. Mermet, Analysis of glass by UV laser ablation inductively coupled plasma atomic emission spectrometry. Part 1. Effect of the laser parameters on the amount of ablated material and the temporal behaviour of the signal for different types of laser, Spectrochim. Acta Part B 51 (1996) 321–332.

[5] M. Ducreux-Zappa, J.M. Mermet, Analysis of glass by UV laser ablation inductively coupled plasma atomic emission spectrometry. Part 2. Analytical figures of merit, Spectrochim. Acta Part B 51 (1996) 334–341.

[6] M. Hemmerlin, J.M. Mermet, M. Bertucci, P. Zydowicz, Determination of additives in PVC material by UV laser ablation inductively coupled plasma atomic emission spectrometry, Spectrochim. Acta Part B 51 (1997) 421–430.

[7] V. Kanicky, V. Otruba, J.M. Mermet, Analysis of tungsten carbide coatings by UV laser ablation inductively coupled plasma atomic emission spectrometry, Spectrochim. Acta Part B 55 (2000) 575–586.
[8] P. Musil, V. Otruba, V. Kanicky, J.M. Mermet, Determination of elements in agricultural soils using IR laser ablation inductively coupled plasma atomic emission spectrometry, Spectrochim. Acta Part B 55 (2000) 1747–1758.
[9] A.M. Ghazi, S. Shuttleworth, Trace element determination of single fluid inclusions by laser ablation ICP-MS: applications for halites from sedimentary basins, Analyst 125 (2000) 205–210.
[10] Z. Chen, D. Canil, H.P. Longerich, Automated in situ trace element analysis of silicate materials by laser ablation inductively coupled plasma mass spectrometry, Fresenius J. Anal. Chem. 368 (2000) 73–78.
[11] C. Pickhardt, I.B. Brenner, J.S. Becker, H.I. Dietze, Determination of trace elements in zeolites by laser ablation ICP-MS, Fresenius J. Anal. Chem. 368 (2000) 79–87.
[12] D. Bleiner, A. Plotnikov, C. Vogt, K. Wetzig, D. Gunther, Depth profile analysis of various titanium based coatings on steel and tungsten carbide using laser ablation inductively coupled plasma—'time of flight' mass spectrometry, Fresenius J. Anal. Chem. 368 (2000) 221–226.
[13] W. Devos, M.S. Lunder, C. Moor, C. Salter, Laser ablation inductively coupled plasma mass spectrometry (LA-ICP-MS) for spatially resolved trace analysis of early-medieval archaeological iron finds, Fresenius J. Anal. Chem. 366 (2000) 873–880.
[14] F. Li, M.K. Balazs, R. Pong, Total dose measurement for ion implantation using laser ablation ICP-MS, J. Anal. At. Spectrom. 15 (2000) 1139–1141.
[15] H. Toland, B. Perkins, N. Pearce, F. Keenan, M.J. Leng, A study of sclerochronology by laser ablation ICP-MS, J. Anal. At. Spectrom. 15 (2000) 1143–1148.
[16] R. Ma, I. Staton, C.W. Mcleod, M.B. Gomez, M.M. Gomez, M.A. Palacios, Assessment of airborne platinum contamination via ICP-mass spectrometric analysis of tree bark, J. Anal. At. Spectrom. 16 (2001) 1070–1075.
[17] D. Gunther, B. Hattendorf, A. Audetat, Multi-element analysis of melt and fluid inclusions with improved detection capabilities for Ca and Fe using laser ablation with a dynamic reaction cell ICP-MS, J. Anal. At. Spectrom. 16 (2001) 1085–1090.
[18] A. Plotnikov, C. Vogt, V. Hoffmann, C. Taschner, K. Wetzig, Application of laser ablation inductively coupled plasma quadruple mass spectrometry (LA-ICP-MS) for depth profile analysis, J. Anal. At. Spectrom. 16 (2001) 1290–1295.
[19] P.R.D. Mason, A.J.G. Mank, Depth-resolved analysis in multi-layered glass and materials using laser ablation inductively coupled plasma mass spectrometry (LA-ICP-MS), J. Anal. At. Spectrom. 16 (2001) 1381–1388.
[20] X.L. Mao, W.T. Chan, R.E. Russo, Influence of sample surface condition on chemical analysis using laser ablation inductively coupled plasma atomic emission spectroscopy, Appl. Spectrosc. 51 (1997) 1047–1054.
[21] X.L. Mao, A.C. Ciocan, R.E. Russo, Preferential vaporization during laser ablation inductively coupled plasma atomic emission spectroscopy, Appl. Spectrosc. 52 (1998) 913–918.
[22] M. Hemmerlin, J.M. Mermet, Effect of the chemical form of the additives in poly(vinyl chloride) and poly(ethylene) materials on laser ablation efficiency using inductively coupled plasma atomic emission spectrometry, Spectrochim. Acta Part B 52 (1997) 1687–1694.
[23] A.C. Ciocan, X.L. Mao, O.V. Borisov, R.E. Russo, Optical emission spectroscopy studies of the influence of laser ablated mass on dry inductively coupled plasma conditions, Spectrochim. Acta Part B 53 (1998) 463–470.
[24] X.L. Mao, O.V. Borisov, R.E. Russo, Enhancement in laser ablation inductively coupled plasma-atomic emission spectrometry based on laser properties and ambient environment, Spectrochim. Acta Part B 53 (1998) 731–739.
[25] R.E. Russo, X.L. Mao, O.V. Borisov, Laser ablation sampling, Trends Anal. Chem. 17 (1998) 461–469.
[26] S.H. Jeong, O.V. Borisov, J.H. Uoo, X.L. Mao, R.E. Russo, Effects of particle size distribution on inductively coupled plasma mass spectrometry signal intensity during laser ablation of glass samples, Anal. Chem. 71 (1999) 5123–5130.
[27] H. Liu, O.V. Borisov, X. Mao, S. Shuttleworth, R.E. Russo, Pb/U fraction during Nd:YAG 213 nm and 266 nm laser ablation sampling with inductively coupled plasma mass spectrometry, Appl. Spectrosc. 54 (2000) 1435–1442.
[28] R.E. Russo, X.L. Mao, O.V. Borisov, H. Liu, Influence of wavelength on fractionation in laser ablation ICP-MS, J. Anal. At. Spectrom. 15 (2000) 1115–1120.
[29] M.M. Heino, P.L. Coustumer, O.F.X. Donard, Micro- and macro-scale investigation of fractionation and matrix effects in LA-ICP-MS at 1064 nm and 266 nm on glassy materials, J. Anal. At. Spectrom. 16 (2001) 542–550.
[30] O.V. Borisov, X.L. Mao, R.E. Russo, Effects of crater development on fractionation and signal intensity during laser ablation inductively coupled plasma mass spectrometry, Spectrochim. Acta Part B 55 (2000) 1693–1704.
[31] M. Sabsabi, P. Cielo, Quantitative analysis of aluminium alloys by laser-induced breakdown spectroscopy and plasma characterization, Appl. Spectrosc. 49 (1995) 499–507.
[32] L.S. Onge, M. Sabsabi, P. Cielo, Quantitative analysis of additives in solid zinc alloys by laser-induced plasma spectrometry, J. Anal. At. Spectrom. 12 (1997) 997–1004.

[33] D.A. Rusak, B.C. Castle, B.W. Smith, J.D. Winefordner, Excitaional, vibrational, and rotational temperatures in Nd:YAG and XeCl laser-induced plasmas, Spectrochim. Acta Part B 52 (1997) 1929–1935.

[34] I.B. Gornushkin, A. Ruiz-Medina, J.M. Anzano, B.W. Smith, J.D. Winefordner, Identification of particulate materials by correlation analysis using a microscopic laser induced breakdown spectrometer, J. Anal. At. Spectrom. 15 (2000) 581–586.

[35] J. Amador-Hernandez, L.E. Garcia-Ayuso, J.M. Fernandez-Romero, M.D. Luque de Castro, Partial least squares regression for problem solving in precision metal analysis by laser breakdown spectrometry, J. Anal. At. Spectrom. 15 (2000) 587–593.

[36] S.R. Goode, S.L. Morgan, R. Hoskins, A. Oxsher, Identifying alloys by laser-induced breakdown spectroscopy with a time-resolved high resolution echelle spectrometer, J. Anal. At. Spectrom. 15 (2000) 1133–1138.

[37] V. Margetic, A. Pakulev, A. Stockhaus, M. Bolshov, K. Niemax, R. Hergenroder, A comparison of nanosecond and femtosecond laser-induced plasma spectroscopy of brass samples, Spectrochim. Acta Part B 55 (2000) 1771–1785.

[38] V. Margetic, M. Bolshov, A. Stockhaus, K. Niemax, R. Hergenroder, Depth profiling of multi-layer samples using femtosecond laser ablation, J. Anal. At. Spectrom. 16 (2001) 616–621.

[39] M.P. Mateo, J.M. Vadillo, J.J. Laserna, Irradiance-dependent depth profiling of layered materials using laser-induced plasma spectrometry, J. Anal. At. Spectrom. 16 (2001) 1317–1321.

[40] M. Ohata, H. Yasuda, Y. Namai, F. Furuta, Laser ablation inductively coupled plasma mass spectrometry (LA-ICP-MS): comparison of different internal standardization methods using laser-induced plasma (LIP) emission and LA-ICP-MS signals, Anal. Sci., in press..

[41] M. Ohata, N. Furuta, Spatial characterization of emission intensities and temperatures of a high power nitrogen microwave-induced plasma, J. Anal. At. Spectrom. 12 (1997) 341–347.